INTERNATIONAL JOURNAL FOR NUMERICAL METHODS IN ENGINEERING
Int. J. Numer. Meth. Engng 2004; **60**:1–16 *Prepared using* nmeauth.cls *[Version: 2002/09/18 v2.02]*

Rayleigh wave correction for the BEM analysis of two-dimensional elastodynamic problems in a half-space

I. Arias*and J. D. Achenbach

Center for Quality Engineering and Failure Prevention
Northwestern University, Evanston, IL 60208, USA

SUMMARY

A simple, elegant approach is proposed to correct the error introduced by the truncation of the infinite boundary in the BEM modelling of two-dimensional wave propagation problems in elastic half-spaces. The proposed method exploits the knowledge of the far-field asymptotic behavior of the solution to adequately correct the BEM displacement system matrix for the truncated problem to account for the contribution of the omitted part of the boundary. The reciprocal theorem of elastodynamics is used for a convenient computation of this contribution involving the same boundary integrals that form the original BEM system. The method is formulated for a two-dimensional homogeneous, isotropic, linearly elastic half-space and its implementation in a frequency domain boundary element scheme is discussed in some detail. The formulation is then validated for a free Rayleigh pulse travelling on a half-space and successfully tested for a benchmark problem with a known approximation to the analytical solution. Copyright © 2004 John Wiley & Sons, Ltd.

KEY WORDS: Infinite domain; frequency domain BEM; boundary truncation; 2D elastodynamics; Rayleigh waves

1. INTRODUCTION

The boundary element method (BEM) is ideally suited for the numerical analysis of problems of wave propagation in elastic media that are unbounded outside a bounded domain with boundary S, since only the boundary S needs to be discretized and the radiation conditions at infinity are naturally accounted for in the formulation. However, when the elastic medium is modelled as a half-space, with possibly some geometric features such as cracks, voids and inclusions, not only the domain but also its boundary are unbounded. In elastodynamics, the BEM formulation for a half-space is usually stated in terms of full-space – rather than half-space – Green's functions, and thus the discretization over the boundary of the half-space is needed in order to enforce the appropriate boundary conditions. Obviously, the infinite extent of the boundary requires a special treatment in any numerical scheme. This issue has been the object of intense research (see for example Reference [1]).

*Correspondence to: Graduate Aeronautical Laboratories, California Institute of Technology, 1200 E. California Blvd. MC: 205-45, Pasadena, CA 91125, USA. Tel: (626) 3954757, Fax: (626) 4492677, Email:iarias@caltech.edu

The most straightforward approach consists in restricting the discretization to a finite part of the boundary, thereby truncating the boundary integrals. In three dimensional elastodynamics, this approach can lead to accurate solutions near the source region, as long as the computational mesh is extended far enough, since the waves propagating along the boundary, i.e. longitudinal, transverse, and Rayleigh waves, exhibit geometrical attenuation in the direction of propagation. Thus, the contribution to the integrals from regions far away from the zone of interest is negligible. However, in a two-dimensional geometry, Rayleigh surface waves propagate along the boundary without attenuation, and therefore the above approach will produce inaccurate results due to spurious reflections from the ends of the computational mesh. This difficulty has been traditionally overcome in the frequency domain by adding a small amount of damping to the material, which results in attenuation of all types of waves. This approach provides accurate solutions when the truncation points are at sufficient distances from the region of interest [2], which leads to an inefficient use of the computational resources.

A more efficient and sophisticated treatment of the infinite boundary is provided by the infinite boundary element technique first proposed by Watson [3] and later presented in more detailed form in Reference [4]. This technique maps the omitted part of the boundary, which extends to infinity, into a finite region. The behavior of the displacements and the tractions in the infinite region is modelled through decay functions suitable for each particular problem. Zhang *et al* [5] developed decay shape functions to describe three-dimensional far-field wave propagation based on the asymptotic behavior of Stokes' solutions. Bu [6] proposed an oscillatory shape function derived from three-dimensional Rayleigh wave propagation in the far-field. In all cases, the resulting integrals over the infinite element require special numerical integration schemes and are quite involved particulary for the case of oscillatory kernels.

In this paper, we present a simple, elegant approach to the treatment of infinite boundaries for time-harmonic problems. The formulation is detailed for a two-dimensional, homogeneous, isotropic, linearly elastic half-space in which the main objective is to allow the undamped Rayleigh waves to propagate to infinity. The proposed method consists of two parts.

First, common to other techniques, the knowledge of the general form of the asymptotic far-field solution is exploited. For instance, in Reference [7], when dealing with waves propagating in channels, a fictitious boundary is introduced to close the unbounded domain and the knowledge of the far field standing wave solutions is used to derive appropriate Robin boundary conditions. The derivation of this type of absorbing boundary conditions is not obvious in many applications. In the present paper, it is assumed that the numerical solution takes the known far-field general form of Rayleigh waves in the omitted part of the boundary, in principle, of unknown amplitude and phase. This assumption is used here to rewrite the integrals that represent the contribution of the omitted part or the boundary as the product of integrals of known quantities on the omitted part of the boundary and the unknown amplitudes and phases of the far-field Rayleigh waves. In order to eliminate these unknowns, the assumed far-field Rayleigh waves are matched to the nodal values at the end nodes of the computational boundary. Consequently, the coefficients of the original BEM displacement system matrix associated with the end nodes are modified.

Next, the integrals on the infinite omitted part of the boundary are computed. These integrals may be approximated numerically, as has been done in some applications of the infinite boundary element method [6]. Also, in References [8, 9], which address the problem of soil amplification of seismic waves, the contribution of the completely known far field solution (given as data in these papers) is integrated numerically over the infinite part of the boundary.

By contrast, in the present paper the reciprocity theorem of elastodynamics is invoked to derive a boundary integral representation for the known general form of the far-field solution, i.e. the unit amplitude Rayleigh wave, with the same fundamental solution of the original formulation [10]. This representation involves the same integrals over the omitted part of the boundary that are needed to modify the original BEM system, integrals of known quantities on the originally discretized part of the boundary, and in some cases integrals on additional boundaries whose computational cost is very small. This simple approach provides a convenient way of computing the integrals over the omitted part of the boundary in terms of integrals on finite boundaries. Furthermore, it allows for a very efficient numerical implementation in terms of the same basic element integrals of the original BEM scheme. Consequently, the proposed technique comes at a very low, in many cases essentially negligible, additional cost as compared to the simple truncation of the boundary.

It should be noted that for the present method to be accurate, the discretized boundary needs to be extended far enough for the body waves to have substantially attenuated and thus, for the assumption that the Rayleigh waves dominate the solution in the omitted part of the boundary to hold. In return, no spurious reflections are produced, and the accuracy of the solution is not degraded near the ends of the mesh.

The method is developed in detail for Rayleigh waves in two-dimensional elastodynamics, but the basic ideas are applicable to a broader range of wave propagation problems. The best suited problems are those in which the far-field solution does not decay, such as Stoneley waves in material interfaces, or propagating Lamb modes in layers. However, it can also be useful for cases of decaying far-field solutions, such as occur in two-dimensional viscoelasticity. In this case, although the Rayleigh waves attenuate, they do so slower than the body waves, and consequently the present technique can reduce the extent of the computational mesh.

In the following sections, the above described techniques are first formulated and their implementation in a frequency domain boundary element scheme is discussed. Then, the proposed method is validated for a free Rayleigh wave travelling on a half-space and tested for a benchmark problem with a known asymptotic approximation to the analytical solution.

2. FORMULATION

2.1. Reciprocity theorem in time-harmonic elastodynamics

The dynamic reciprocity theorem relates two elastodynamic states of the same bounded or unbounded body [11]. These states are defined by sets of displacements and stresses which are the solution to two elastodynamic boundary value problems for the same body but with possibly different distributions of body forces, different initial conditions and different boundary conditions. For time-harmonic two-dimensional elastodynamics it can be stated as follows. Let Ω be an elastic region with boundary Γ and closure $\overline{\Omega}$. Consider two time-harmonic elastodynamic states of the same angular frequency ω on $\overline{\Omega}$ denoted with superscripts A and B, respectively. Then,

$$\begin{aligned}&\int_{\Omega}\left[f_{\alpha}^{A}(\mathbf{x},\omega)u_{\alpha}^{B}(\mathbf{x},\omega)-f_{\alpha}^{B}(\mathbf{x},\omega)u_{\alpha}^{A}(\mathbf{x},\omega)\right]d\Omega(\mathbf{x})\\&=\int_{\Gamma}\left[\sigma_{\beta\alpha}^{B}(\mathbf{x},\omega)u_{\alpha}^{A}(\mathbf{x},\omega)-\sigma_{\beta\alpha}^{A}(\mathbf{x},\omega)u_{\alpha}^{B}(\mathbf{x},\omega)\right]n_{\beta}(\mathbf{x})d\Gamma(\mathbf{x}),\end{aligned}\tag{1}$$

where $f_\alpha^{A,B}$, $u_\alpha^{A,B}$, $\sigma_{\beta\alpha}^{A,B}$ represent body forces, displacements and stresses, respectively, and $\mathbf{n}$ is the unit vector along the outward normal to Γ.

In the formulation of the boundary element method, Eq. (1) is invoked to derive an integral representation for the displacement solution of the problem to be solved (state A) at a point $\boldsymbol{\xi} \in \Omega$ by choosing the time-harmonic fundamental solution, i.e. the solution to a time-harmonic unit point load applied at $\boldsymbol{\xi}$, as elastodynamic state B. Then, a limiting process is followed to derive a boundary integral equation for points located on the boundary, i.e. $\boldsymbol{\xi} \in \Gamma$ [2]. In this paper, the reciprocity theorem is invoked a second time to obtain an integral representation for the contribution of the omitted part of the boundary as described in section 2.4.

2.2. Asymptotic behavior of the displacement far-field solution

Let us consider a two-dimensional elastodynamic problem defined on a homogeneous, isotropic, linearly elastic half-space with boundary Γ. The corresponding frequency domain boundary integral equation for a point $\boldsymbol{\xi} \in \Gamma$ in the absence of body forces may be obtained from Eq. (1) as

$$c_{\alpha\beta}(\boldsymbol{\xi})\, u_\beta(\boldsymbol{\xi},\omega) = \int_\Gamma \left[u^*_{\alpha\beta}(\boldsymbol{\xi},\mathbf{x},\omega)\, t_\beta(\mathbf{x},\omega) - t^*_{\alpha\beta}(\boldsymbol{\xi},\mathbf{x},\omega)\, u_\beta(\mathbf{x},\omega)\right] d\Gamma(\mathbf{x}), \quad \alpha,\beta = 1,2, \quad (2)$$

where $u^*_{\alpha\beta}$ and $t^*_{\alpha\beta}$ are the full-space frequency domain elastodynamic fundamental solution displacement and traction tensors respectively [2]. Note that $u^*_{\alpha\beta}(\boldsymbol{\xi},\mathbf{x},\omega)$ and $t^*_{\alpha\beta}(\boldsymbol{\xi},\mathbf{x},\omega)$ represent the "β" component of the displacement and the traction on the boundary, respectively, at the point $\mathbf{x}$ due to a unit time-harmonic load of angular frequency ω applied at the point $\boldsymbol{\xi}$ in the direction "α". Also, u_β, t_β are frequency domain displacements and tractions on the boundary, ω stands for the angular frequency and $c_{\alpha\beta}$ is called the jump coefficient given by:

$$c_{\alpha\beta}(\boldsymbol{\xi}) = \begin{cases} \frac{1}{2}\delta_{\alpha\beta}, & \text{if } \Gamma \text{ is smooth at point } \boldsymbol{\xi}, \\ c_{\alpha\beta}, & \text{if } \Gamma \text{ has a corner at point } \boldsymbol{\xi}, \end{cases} \quad (3)$$

where $\delta_{\alpha\beta}$ represents the Kronecker delta. The jump coefficient for corner points can be derived by an indirect approach as described in Reference [2]. The integrals in Eq. (2) are interpreted in the sense of the Cauchy Principal Value.

Let us assume that outside a localized region, Γ_1, where the boundary may be irregular and subjected to various types of boundary conditions, the boundary is a straight surface free of tractions. Let Γ_0 be the part of this traction-free boundary which will be included in the discretization and Γ_∞ the remaining infinite part which will be omitted (see Fig. 1). In this case, Eq. (2) becomes

$$\begin{aligned} c_{\alpha\beta}(\boldsymbol{\xi})\, u_\beta(\boldsymbol{\xi},\omega) + \int_{\Gamma_\infty} t^*_{\alpha\beta}(\boldsymbol{\xi},\mathbf{x},\omega)\, u_\beta(\mathbf{x},\omega) d\Gamma(\mathbf{x}) + \\ \int_{\Gamma_0 \bigcup \Gamma_1} t^*_{\alpha\beta}(\boldsymbol{\xi},\mathbf{x},\omega)\, u_\beta(\mathbf{x},\omega) d\Gamma(\mathbf{x}) = \int_{\Gamma_1} u^*_{\alpha\beta}(\boldsymbol{\xi},\mathbf{x},\omega)\, t_\beta(\mathbf{x},\omega) d\Gamma(\mathbf{x}). \end{aligned} \quad (4)$$

The three characteristic waves along the traction-free boundary, namely the longitudinal, transverse, and Rayleigh waves, all contribute to the displacement field. However, it is well known that body waves exhibit geometrical decay in the propagating direction, whereas Rayleigh waves in two dimensions do not. Therefore, the displacement far-field solution can

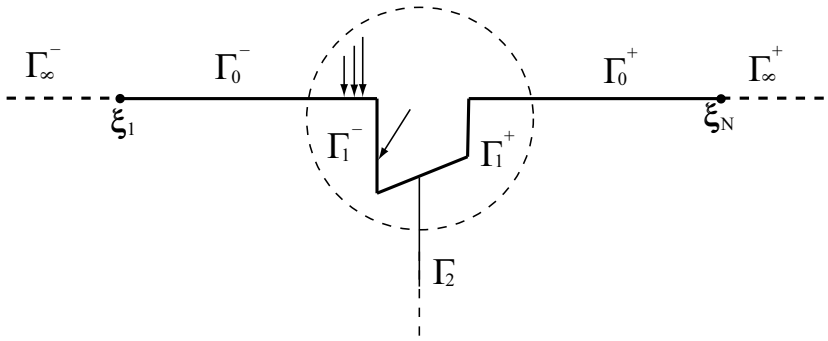

Figure 1. Schematic definition of the computational domain, with $\Gamma^{\pm} = \Gamma_\infty^{\pm} \bigcup \Gamma_0^{\pm} \bigcup \Gamma_1^{\pm}$ and $\Gamma_i = \Gamma_i^+ \bigcup \Gamma_i^-$.

be approximated by the Rayleigh surface wave component of the solution, thereby neglecting the contribution of the body waves. Hence, if the truncation points $\boldsymbol{\xi}_1$ and $\boldsymbol{\xi}_N$ are located far enough from the source region, then we can write for each side of the infinite boundary ($\Gamma_\infty^{\pm}$)

$$\begin{aligned} \boldsymbol{\xi} \in \Gamma_\infty^- :\ u_\alpha(\boldsymbol{\xi},\omega) &\approx R^-(\omega)\, u_\alpha^{SR}(\boldsymbol{\xi},\omega), \\ \boldsymbol{\xi} \in \Gamma_\infty^+ :\ u_\alpha(\boldsymbol{\xi},\omega) &\approx R^+(\omega)\, u_\alpha^{SR}(\boldsymbol{\xi},\omega), \end{aligned} \tag{5}$$

where R^- and R^+ are the unknown complex amplitudes of the far-field Rayleigh waves at each side of the boundary and u_α^{SR} represents the frequency domain displacements corresponding to unit amplitude time-harmonic Rayleigh surface waves of angular frequency ω propagating along the surface of the half-space in the positive direction (to the right in Fig. 1). Note that the fact that the far field solution in the boundary extending to $-\infty$ propagates in the negative direction will be taken into account in the complex coefficient R^-. The expressions for u_α^{SR} can be found, for instance, in Reference [12].

Hence, Eq. (2) can be rewritten as:

$$\begin{aligned} &R^-(\omega) \int_{\Gamma_\infty^-} t_{\alpha\beta}^*(\boldsymbol{\xi},\mathbf{x},\omega)\, u_\beta^{SR}(\mathbf{x},\omega) d\Gamma(\mathbf{x}) + R^+(\omega) \int_{\Gamma_\infty^+} t_{\alpha\beta}^*(\boldsymbol{\xi},\mathbf{x},\omega)\, u_\beta^{SR}(\mathbf{x},\omega) d\Gamma(\mathbf{x}) \\ &+ c_{\alpha\beta}(\boldsymbol{\xi})\, u_\beta(\boldsymbol{\xi},\omega) + \int_{\Gamma_0 \bigcup \Gamma_1} t_{\alpha\beta}^*(\boldsymbol{\xi},\mathbf{x},\omega)\, u_\beta(\mathbf{x},\omega) d\Gamma(\mathbf{x}) = \int_{\Gamma_1} u_{\alpha\beta}^*(\boldsymbol{\xi},\mathbf{x},\omega)\, t_\beta(\mathbf{x},\omega) d\Gamma(\mathbf{x}). \end{aligned} \tag{6}$$

Note that in Eq. (6) the complex amplitudes R^- and R^+ are unknown, but the integrands over the infinite boundaries Γ_∞^- and Γ_∞^+ are known. Therefore, these integrals may be approximated numerically. Here, however, we propose a more elegant approach based on the reciprocity theorem of elastodynamics. This approach is described in detail in section 2.4.

2.3. Matching with the far-field solution at the ends of the computational boundary

By the use of Eq. (5) the solution is described asymptotically as a Rayleigh wave of unknown amplitude and phase. In order to eliminate the unknowns R^- and R^+ in Eq. (6), the solution in the computational domain is matched to the far-field solution at the end points, i.e. $\boldsymbol{\xi}_1$ and

$\boldsymbol{\xi}_N$. Hence, Eq. (5) yields, in particular:

$$R^-(\omega) \approx \frac{u_\alpha(\boldsymbol{\xi}_1,\omega)}{u_\alpha^{SR}(\boldsymbol{\xi}_1,\omega)}, \quad R^+(\omega) \approx \frac{u_\alpha(\boldsymbol{\xi}_N,\omega)}{u_\alpha^{SR}(\boldsymbol{\xi}_N,\omega)}, \quad \alpha = 1,2. \tag{7}$$

From Eq. (6) we can define:

$$A_\alpha^+(\boldsymbol{\xi},\omega) = \frac{1}{u_\alpha^{SR}(\boldsymbol{\xi}_N,\omega)} \int_{\Gamma_\infty^+} t_{\alpha\beta}^*(\boldsymbol{\xi},\mathbf{x},\omega)\, u_\beta^{SR}(\mathbf{x},\omega) d\Gamma(\mathbf{x}), \quad \alpha = 1,2. \tag{8}$$

Similarly, we can define $A_\alpha^-(\boldsymbol{\xi},\omega)$ using $\boldsymbol{\xi}_1$ and Γ_∞^- instead of $\boldsymbol{\xi}_N$ and Γ_∞^+. With these definitions, Eq. (6) can be rewritten as:

$$\begin{aligned} &c_{\alpha\beta}(\boldsymbol{\xi})\, u_\beta(\boldsymbol{\xi},\omega) + A_\alpha^-(\boldsymbol{\xi},\omega) u_\alpha(\boldsymbol{\xi}_1,\omega) + A_\alpha^+(\boldsymbol{\xi},\omega) u_\alpha(\boldsymbol{\xi}_N,\omega) \\ &+ \int_{\Gamma_0 \bigcup \Gamma_1} t_{\alpha\beta}^*(\boldsymbol{\xi},\mathbf{x},\omega)\, u_\beta(\mathbf{x},\omega) d\Gamma(\mathbf{x}) = \int_{\Gamma_1} u_{\alpha\beta}^*(\boldsymbol{\xi},\mathbf{x},\omega)\, t_\beta(\mathbf{x},\omega) d\Gamma(\mathbf{x}), \quad \alpha = 1,2. \end{aligned} \tag{9}$$

It is convenient to cast Eq. (9) in matrix form as follows:

$$\begin{aligned} &\mathbf{A}^-(\boldsymbol{\xi},\omega)\mathbf{u}(\boldsymbol{\xi}_1,\omega) + \mathbf{A}^+(\boldsymbol{\xi},\omega)\mathbf{u}(\boldsymbol{\xi}_N,\omega) \\ &+ \mathbf{c}(\boldsymbol{\xi})\, \mathbf{u}(\boldsymbol{\xi},\omega) + \int_{\Gamma_0 \bigcup \Gamma_1} \mathbf{t}^*(\boldsymbol{\xi},\mathbf{x},\omega)\, \mathbf{u}(\mathbf{x},\omega) d\Gamma(\mathbf{x}) = \int_{\Gamma_1} \mathbf{u}^*(\boldsymbol{\xi},\mathbf{x},\omega)\, \mathbf{t}(\mathbf{x},\omega) d\Gamma(\mathbf{x}), \end{aligned} \tag{10}$$

where:

$$\mathbf{A}^\pm(\boldsymbol{\xi},\omega) = \begin{bmatrix} A_1^\pm(\boldsymbol{\xi},\omega) & 0 \\ 0 & A_2^\pm(\boldsymbol{\xi},\omega) \end{bmatrix}. \tag{11}$$

It should be noted that Eq. (10) without the first two terms corresponds to the standard simply truncated boundary integral equation. The first two terms represent the correction which accounts for the contribution of the omitted part of the boundary of the half-space on which a Rayleigh surface wave is assumed to be predominant.

2.4. Integral over the omitted part of the infinite boundary

Let us consider a time-harmonic Rayleigh surface wave of angular frequency ω and unit amplitude propagating along the free surface of the half-space in the positive direction. In order to be able to determine the integrals over Γ_∞^- and Γ_∞^+ independently, a multidomain approach is needed in general. Let Γ_2 be a fictitious boundary which divides the half-space into two quarter-spaces and $\Gamma^\pm$ the parts of the boundary Γ contained in each quarter-space, respectively. Let us now choose the time-harmonic Rayleigh surface wave as elastodynamic state A and the time-harmonic full-space fundamental solution of the same frequency ω as elastodynamic state B. By virtue of the reciprocity theorem of elastodynamics stated in Eq (1), and after the limiting process of taking the relation to the boundary, an integral representation is derived for each quarter-space. For instance, for the quarter-space on the positive side of the horizontal axis, i.e. $\boldsymbol{\xi} \in \Gamma^+$ the integral representation is given as:

$$c_{\alpha\beta}(\boldsymbol{\xi})\, u_\beta^{SR}(\boldsymbol{\xi},\omega) = \int_{\Gamma_2 \bigcup \Gamma^+} \left[u_{\alpha\beta}^*(\boldsymbol{\xi},\mathbf{x},\omega)\, t_\beta^{SR}(\mathbf{x},\omega) - t_{\alpha\beta}^*(\boldsymbol{\xi},\mathbf{x},\omega)\, u_\beta^{SR}(\mathbf{x},\omega) \right] d\Gamma(\mathbf{x}). \tag{12}$$

Invoking the zero traction boundary conditions along Γ_0^+ and Γ_∞^+, Eq. (12) becomes:

$$\begin{aligned}\int_{\Gamma_\infty^+} t^*_{\alpha\beta}(\boldsymbol{\xi},\mathbf{x},\omega)\, u^{SR}_\beta(\mathbf{x},\omega)d\Gamma(\mathbf{x}) &= -c_{\alpha\beta}(\boldsymbol{\xi})\, u^{SR}_\beta(\boldsymbol{\xi},\omega)\\ -\int_{\Gamma_0^+ \bigcup \Gamma_1^+ \bigcup \Gamma_2} t^*_{\alpha\beta}(\boldsymbol{\xi},\mathbf{x},\omega)\, u^{SR}_\beta(\mathbf{x},\omega)d\Gamma(\mathbf{x}) &+ \int_{\Gamma_1^+ \bigcup \Gamma_2} u^*_{\alpha\beta}(\boldsymbol{\xi},\mathbf{x},\omega)\, t^{SR}_\beta(\mathbf{x},\omega)d\Gamma(\mathbf{x}).\end{aligned} \tag{13}$$

Thus, Eq. (8) yields:

$$\begin{aligned}u^{SR}_\alpha(\boldsymbol{\xi}_N,\omega)A^+_\alpha(\boldsymbol{\xi},\omega) = -c_{\alpha\beta}(\boldsymbol{\xi})\, u^{SR}_\beta(\boldsymbol{\xi},\omega) &- \int_{\Gamma_0^+ \bigcup \Gamma_1^+ \bigcup \Gamma_2} t^*_{\alpha\beta}(\boldsymbol{\xi},\mathbf{x},\omega)\, u^{SR}_\beta(\mathbf{x},\omega)d\Gamma(\mathbf{x})\\ &+ \int_{\Gamma_1^+ \bigcup \Gamma_2} u^*_{\alpha\beta}(\boldsymbol{\xi},\mathbf{x},\omega)\, t^{SR}_\beta(\mathbf{x},\omega)d\Gamma(\mathbf{x}), \quad \alpha = 1,2.\end{aligned} \tag{14}$$

An analogous equation can be derived for A^-_α, by considering the boundaries of the quarter-space on the negative side of the horizontal axis, i.e. Γ_0^-, Γ_1^- and Γ_2.

Note that the fictitious boundary Γ_2 is, in principle, infinite. However, since the integrand decays rapidly away form the surface of the half-space, the integration can be truncated at a relatively short distance from the surface without loss of accuracy. In fact, it is well known that Rayleigh surface waves penetrate into a material up to a distance of about one wavelength. This can serve as a guiding criterion for the required length of integration.

Note also that if a quarter-space is analyzed, for instance invoking the symmetry of the problem under consideration, the boundary Γ_2 is already present in the formulation as part of Γ_1^+ or Γ_1^-. Obviously, in this case only one of the correction terms in Eq. (10) is necessary.

The key in the present approach is that, by virtue of reciprocity, the integrals extending to infinity in Eq. (10) – which are implicit in $\mathbf{A}^-$ and $\mathbf{A}^+$ through Eq. (11) – and Eq. (8) and its analogous for A^-_α, can be computed by the use of Eq. (14) and its analogous for A^-_α in terms of integrals over the bounded boundaries of the problem and possibly an additional boundary which can be truncated without loss of accuracy. This provides a simple way of calculating the correction to account for the omitted part of the boundary represented by the first two terms in Eq. (10).

3. NUMERICAL IMPLEMENTATION

According to Eq. (10), the computational boundary that needs to be discretized is $\Gamma_0 \bigcup \Gamma_1$. In addition, in order to obtain the correction coefficients $A^\pm_\alpha(\boldsymbol{\xi},\omega)$ two integrations along the fictitious boundary Γ_2 need to be performed.

The BEM system of equations is formed in the usual manner. After the discretization of the domain and the interpolation of the displacements and tractions, the discretized BIE may be written for each node $\boldsymbol{\xi}_j$, N being the total number of nodes, as:

$$\begin{aligned}\mathbf{c}_j\, \mathbf{u}_j(\omega) + \mathbf{A}^-_j(\omega)\mathbf{u}_1(\omega) + \mathbf{A}^+_j(\omega)\mathbf{u}_N(\omega) + \sum_{e\in B_0 \bigcup B_1}\sum_{k=1}^{N_e}\left\{\int_{\Gamma_e} \mathbf{t}^*(\boldsymbol{\xi}_j,\eta,\omega)\, \boldsymbol{\phi}_k(\eta)d\Gamma(\eta)\right\}\mathbf{u}_k(\omega)\\ = \sum_{e\in B_1}\sum_{k=1}^{N_e}\left\{\int_{\Gamma_e} \mathbf{u}^*(\boldsymbol{\xi}_j,\eta,\omega)\, \boldsymbol{\phi}_k(\eta)d\Gamma(\eta)\right\}\mathbf{t}_k(\omega), \quad j = 1,N,\end{aligned} \tag{15}$$

where $\mathbf{c}_j = \mathbf{c}(\boldsymbol{\xi}_j)$ and $\mathbf{A}_j^{\pm}(\omega) = \mathbf{A}^{\pm}(\boldsymbol{\xi}_j, \omega)$ and, similarly, $\mathbf{u}_j$ and $\mathbf{t}_j$ are displacements and tractions at node $\boldsymbol{\xi}_j$, respectively. Here, B_i is the set of elements corresponding to Γ_i, N_e is the number of nodes per element, $\boldsymbol{\phi}_k$ are 2 x 2 diagonal matrices containing the corresponding shape functions ϕ_k, and $\eta \in [-1, 1]$ represents the intrinsic coordinate of the parent element.

Following the notation in Reference [2], we can define:

$$\hat{\mathbf{H}}^e_{jk}(\omega) = \int_{\Gamma_e} \mathbf{t}^*(\boldsymbol{\xi}_j, \eta, \omega)\, \boldsymbol{\phi}_k(\eta) d\Gamma(\eta), \tag{16}$$

$$\mathbf{G}^e_{jk}(\omega) = \int_{\Gamma_e} \mathbf{u}^*(\boldsymbol{\xi}_j, \eta, \omega)\, \boldsymbol{\phi}_k(\eta) d\Gamma(\eta), \tag{17}$$

which are 2 x 2 matrices that relate the collocation point $\boldsymbol{\xi}_j$ with the node k of element e. Then, Eq. (15) can be rewritten as:

$$\begin{aligned} &\mathbf{c}_j\, \mathbf{u}_j(\omega) + \mathbf{A}_j^-(\omega)\mathbf{u}_1(\omega) + \mathbf{A}_j^+(\omega)\mathbf{u}_N(\omega) \\ &+ \sum_{e \in B_0 \bigcup B_1} \sum_{k=1}^{N_e} \hat{\mathbf{H}}^e_{jk}(\omega)\mathbf{u}_k(\omega) = \sum_{e \in B_1} \sum_{k=1}^{N_e} \mathbf{G}^e_{jk}(\omega)\mathbf{t}_k(\omega), \quad j = 1, N. \end{aligned} \tag{18}$$

The above equation can be written in a more compact manner by defining:

$$\mathbf{H}^e_{jk}(\omega) = \begin{cases} \hat{\mathbf{H}}^e_{jk}(\omega) & \text{if } j \neq k, \\ \hat{\mathbf{H}}^e_{jk}(\omega) + \mathbf{c}_j & \text{if } j = k. \end{cases} \tag{19}$$

Then, assembling the matrices $\mathbf{H}^e_{jk}$ and $\mathbf{G}^e_{jk}$ into the global matrices $\mathbf{H}$ and $\mathbf{G}$ respectively, and the local vectors $\mathbf{u}_k$ and $\mathbf{t}_k$ into the global vectors $\mathbf{U}$ and $\mathbf{T}$ we can write:

$$\mathbf{H}(\omega)\, \mathbf{U}(\omega) + \begin{bmatrix} \mathbf{A}_1^-(\omega) \\ \vdots \\ \mathbf{A}_N^-(\omega) \end{bmatrix} \begin{bmatrix} u_1(\boldsymbol{\xi}_1, \omega) \\ u_2(\boldsymbol{\xi}_1, \omega) \end{bmatrix} + \begin{bmatrix} \mathbf{A}_1^+(\omega) \\ \vdots \\ \mathbf{A}_N^+(\omega) \end{bmatrix} \begin{bmatrix} u_1(\boldsymbol{\xi}_N, \omega) \\ u_2(\boldsymbol{\xi}_N, \omega) \end{bmatrix} = \mathbf{G}(\omega)\, \mathbf{T}(\omega). \tag{20}$$

From Eq. (20) follows that the $\mathbf{H}$ matrix for the corrected BEM scheme is obtained from the original $\mathbf{H}$ matrix by adequately adding the correction coefficients $\mathbf{A}_j^-$ and $\mathbf{A}_j^+$ to the columns corresponding to the end nodes, $\boldsymbol{\xi}_1$ and $\boldsymbol{\xi}_N$. Thus, the contribution from the omitted part of the boundary can be introduced in the formulation simply by adding to the original $\mathbf{H}$ matrix the following correction matrix:

$$\mathbf{A}(\omega) = \left[\begin{array}{cc|ccccc|cc} A_1^-(\boldsymbol{\xi}_1, \omega) & 0 & \ddots & & \vdots & & & A_1^+(\boldsymbol{\xi}_1, \omega) & 0 \\ 0 & A_2^-(\boldsymbol{\xi}_1, \omega) & & \ddots & \vdots & & & 0 & A_2^+(\boldsymbol{\xi}_1, \omega) \\ \vdots & \vdots & \cdots & \cdots & 0 & \cdots & \cdots & \vdots & \vdots \\ A_1^-(\boldsymbol{\xi}_N, \omega) & 0 & & & \vdots & \ddots & & A_1^+(\boldsymbol{\xi}_N, \omega) & 0 \\ 0 & A_2^-(\boldsymbol{\xi}_N, \omega) & & & \vdots & & \ddots & 0 & A_2^+(\boldsymbol{\xi}_N, \omega) \end{array}\right]. \tag{21}$$

Hence, the corrected BEM system may be written as:

$$[\mathbf{H}(\omega) + \mathbf{A}(\omega)]\, \mathbf{U}(\omega) = \mathbf{G}(\omega)\, \mathbf{T}(\omega). \tag{22}$$

Equation (22) constitutes the BEM system modified to account for the contribution of the far-field Rayleigh surface wave through the correction matrix $\mathbf{A}(\omega)$. In the following, we propose a technique to compute the coefficients of the correction matrix by interpolating the known displacements and tractions of the Rayleigh wave far-field solution with the same element shape functions implemented in the BEM scheme. Conveniently, this approximation allows for the correction coefficients to be computed with the same element matrices used to compute the original $\mathbf{H}$ and $\mathbf{G}$ matrices. Let us consider the correction $\mathbf{A}_j^+$ first. By interpolating $\mathbf{u}^{SR}$ and $\mathbf{t}^{SR}$ with the shape functions ϕ_k, Eq. (14) can be rewritten as:

$$\begin{aligned} u_\alpha^{SR}(\boldsymbol{\xi}_N,\omega)A_\alpha^+(\boldsymbol{\xi}_j,\omega) = -c_{\alpha\beta}(\boldsymbol{\xi}_j)\, u_\beta^{SR}(\boldsymbol{\xi}_j,\omega) \\ - \sum_{e\in B_0^+ \bigcup B_1^+ \bigcup B_2} \sum_{k=1}^{N_e} \left\{ \int_{\Gamma_e} t^*_{\alpha\beta}(\boldsymbol{\xi}_j,\eta,\omega)\, \phi_k(\eta) d\Gamma(\eta) \right\} u_\beta^{SR}(\boldsymbol{\xi}_k,\omega) \\ + \sum_{e\in B_1^+ \bigcup B_2^+} \sum_{k=1}^{N_e} \left\{ \int_{\Gamma_e} u^*_{\alpha\beta}(\boldsymbol{\xi}_j,\eta,\omega)\, \phi_k(\eta) d\Gamma(\eta) \right\} t_\beta^{SR}(\boldsymbol{\xi}_k,\omega), \\ j=1,N \quad \alpha=1,2, \end{aligned} \tag{23}$$

and, recalling the definitions in Eqs. (16) and (17), we can write:

$$\begin{aligned} \mathbf{A}_j^+(\omega)\mathbf{u}_N^{SR}(\omega) = -\mathbf{c}_j\, \mathbf{u}_j^{SR}(\omega) - \sum_{e\in B_0^+ \bigcup B_1^+} \sum_{k=1}^{N_e} \hat{\mathbf{H}}^e_{jk}(\omega)\mathbf{u}_k^{SR}(\omega) - \sum_{e\in B_2} \sum_{k=1}^{N_e} \hat{\mathbf{H}}^e_{jk}(\omega)\mathbf{u}_k^{SR}(\omega) \\ + \sum_{e\in B_1^+} \sum_{k=1}^{N_e} \mathbf{G}^e_{jk}(\omega)\mathbf{t}_k^{SR}(\omega) + \sum_{e\in B_2} \sum_{k=1}^{N_e} \mathbf{G}^e_{jk}(\omega)\mathbf{t}_k^{SR}(\omega), \\ j=1,N. \end{aligned} \tag{24}$$

Note that the fictitious boundary Γ_2 has been introduced in order compute the correction for each truncation point, $\boldsymbol{\xi}_1$ and $\boldsymbol{\xi}_N$, independently. Thus, the collocation point $\boldsymbol{\xi}_j$ never lies on Γ_2 and consequently, the integrands involved in the computation of the additional matrices $\hat{\mathbf{H}}^e_{jk}$ and $\mathbf{G}^e_{jk}$ for $e \in B_2$ are never singular. It should be pointed out as well that the discretization of Γ_2 does not add degrees of freedom to the final BEM system of equations. Thus, the size of the modified BEM system in Eq. (22) is exactly the same as the original one.

Let us consider the assembly of the elements corresponding to the original boundary Γ^+ and the additional fictitious boundary Γ_2 independently. So, for elements and nodes that lie on Γ^+, the local element matrices $\mathbf{H}^e_{jk}$ and $\mathbf{G}^e_{jk}$ and the local vectors $\mathbf{u}_k^{SR}$, and $\mathbf{t}_k^{SR}$ are assembled into the global matrices $\mathbf{H}^+$ and $\mathbf{G}^+$ and the global vectors $\mathbf{U}_+^{SR}$ and $\mathbf{T}_+^{SR}$, respectively. Similarly, the local element matrices $\hat{\mathbf{H}}^e_{jk}$ and $\mathbf{G}^e_{jk}$ and the local vectors $\mathbf{u}_k^{SR}$ and $\mathbf{t}_k^{SR}$ corresponding to Γ_2 are assembled into the global matrices $\mathbf{H}_2$ and $\mathbf{G}_2$ and the global vectors $\mathbf{U}_2^{SR}$ and $\mathbf{T}_2^{SR}$, respectively. The the local matrices $\mathbf{A}_j^+$, which are only defined for nodes lying on the original boundary Γ, are assembled into a global matrix $\mathbf{A}^+$. Then, from Eq. (24) yields:

$$\mathbf{A}^+(\omega)\mathbf{u}_N^{SR}(\omega) = -\left[\mathbf{H}^+(\omega) \mid \mathbf{H}_2(\omega)\right] \left[\frac{\mathbf{U}_+^{SR}(\omega)}{\mathbf{U}_2^{SR}(\omega)}\right] + \left[\mathbf{G}^+(\omega) \mid \mathbf{G}_2(\omega)\right] \left[\frac{\mathbf{T}_+^{SR}(\omega)}{\mathbf{T}_2^{SR}(\omega)}\right]. \tag{25}$$

The analogous equation for $\mathbf{A}^-(\omega)$ is derived in a similar manner.

Note that Eq. (25) allows us to compute the coefficients of the correction matrix $\mathbf{A}$ that appears in the modified BEM system in Eq. (22) by employing the same element matrices $\mathbf{H}^e_{jk}$ and $\mathbf{G}^e_{jk}$ that form the original BEM system and some additional but similar ones corresponding to the elements lying on the additional fictitious boundary Γ_2. As previously indicated, the properties of the Rayleigh wave allow for the truncation of this boundary at a distance of a few Rayleigh wavelengths from the surface of the half-space. Thus, the cost of computing the additional element matrices is very low in general. Note also that no special numerical integration scheme is required and the integrals can be computed using the same integration routines implemented in the standard BEM code.

Furthermore, in cases where the symmetry of the problems allows for its restriction to the quarter-space, the fictitious boundary Γ_2 coincides with the also fictitious symmetry boundary and, thus, belongs to the original boundary of the problem defined in the quarter-space. In this situation, no additional element matrix computation is required and the correction to account for the part of the boundary excluded from the discretization can be implemented at essentially no additional cost.

It should be pointed out as well that the above presented implementation is very simple and requires minimum modification of the routine which generates the $\mathbf{H}$ and $\mathbf{G}$ matrices. Once the original matrices are computed in the usual manner, they are used to obtain the correction matrices $\mathbf{A}^{\pm}$ according to Eq. (25). Then the modified matrices are generated as indicated in Eq. (22).

4. NUMERICAL RESULTS

The general formulation presented in the previous section is tested for two different problems. For each problem, the analytical solution is compared to two different BEM solutions. One is obtained by simple truncation of the integrals over Γ_∞, the truncated numerical solution in short. The other BEM solution is obtained by the proposed technique, and is called the corrected numerical solution. Three-node quadratic elements have been used.

In the first problem, a free Rayleigh pulse travelling along a two-dimensional homogeneous, isotropic, linearly elastic half-space is analyzed. This example is intended as a validation of the method, and, since the main assumption exactly holds, very accurate results are expected irrespective of the location of the truncation point. Then, Lamb's problem of a pulse load acting on a half-space with a Gaussian spatial distribution is studied. In this case, both body and Rayleigh waves are excited, and therefore it is representative of engineering applications. From the previous sections, we can anticipate that the corrected solution should be accurate for all times and everywhere in the computational domain, as long as the truncation point is chosen far enough for the body waves to be negligible at this point. In both examples, a quarter-space is analyzed, and therefore the corrected solution has the same computational cost as the truncated solution. The time pulse considered in each of these examples is a sinusoidal signal modulated by a Gaussian function, i.e.

$$g(t) = e^{-\kappa^2 (t-t_0)^2} \sin\left[\Omega(t-t_0)\right], \tag{26}$$

where Ω is the central angular frequency, κ is twice the inverse of the Gaussian radius and t_0 is a time delay with respect to the initial time $t = 0^+$. This type of pulse corresponds to that generated by ultrasonic transducers. The parameters have been chosen for a central frequency

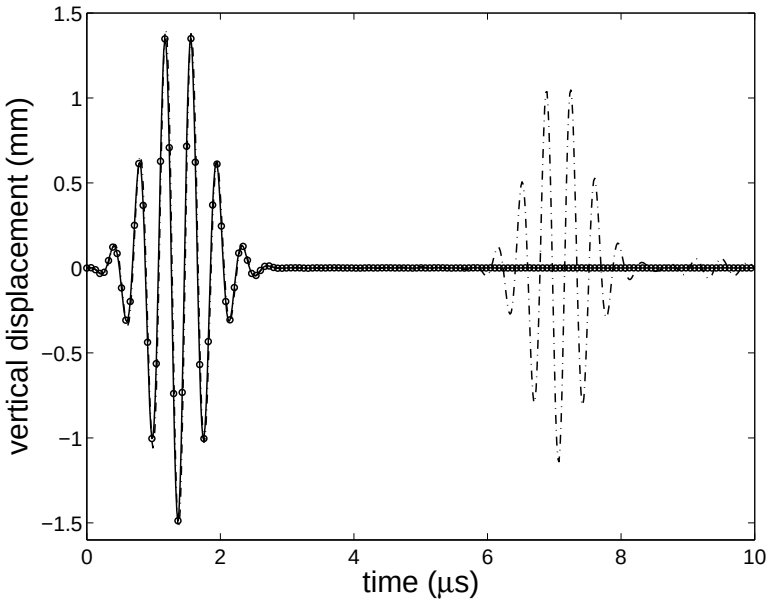

Figure 2. Time signal at $x_1 = 0.5\lambda_R$ (λ_R is the Rayleigh wavelength for the central frequency) for the free Rayleigh pulse problem. The solid line corresponds to the analytical solution. The dashed line and the circles correspond to the truncated and the corrected BEM models, respectively.

of 2.56 MHz. The material properties are those of aluminum and no damping has been taken into account.

4.1. Free Rayleigh pulse problem

Consider a free Rayleigh pulse with the above described temporal distribution propagating along the free surface of a half-space. This wave can be reproduced in the numerical method by considering a quarter-space, and by imposing on the fictitious vertical boundary the known displacements corresponding to the Rayleigh wave. The truncated and corrected numerical schemes are employed to obtain displacements on the free surface, which are then compared to those of the Rayleigh wave. The time domain analytical displacements are obtained by convolution with the pulse.

Both the time and the space discretization have been designed according to the requirements of the central frequency. The sampling of the time signal for the discrete Fourier transform has been designed so that the central period is represented with at least 6 sample points. The element size is selected to have at least 4 elements per Rayleigh wavelength λ_R. Finally, the domain has been truncated at distances of $10\lambda_R$ along the surface and $4\lambda_R$ along the fictitious vertical boundary of the quarter-space. Note that the assumed form of the far-field solution is exactly valid everywhere, since the propagating wave is a Rayleigh wave. Therefore, for this particular case, the corrected results are independent of the location of the truncation point.

Figures 2 and 3 show the time signal at two different locations on the surface, $x_1 = 0.5\lambda_R$ and the truncation point $x_1 = 10\lambda_R$, respectively. For both locations, the time signals of the

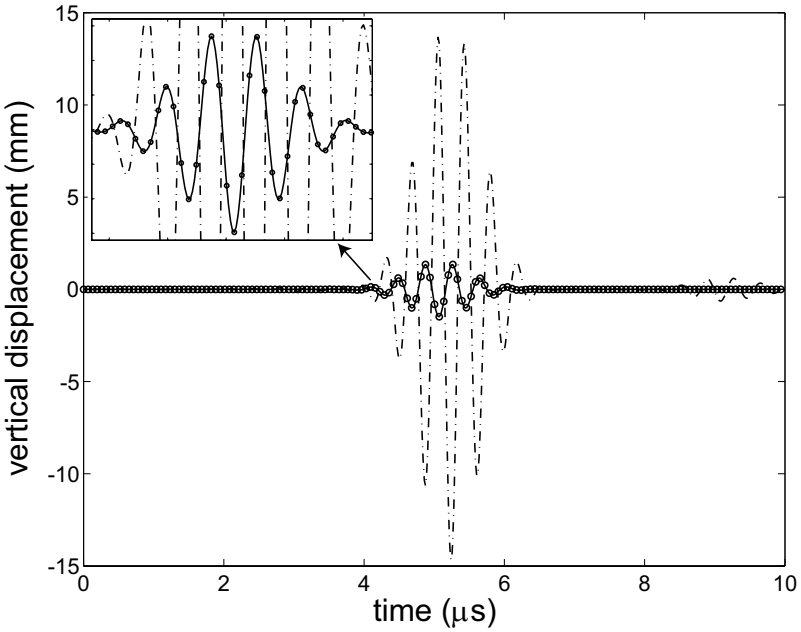

Figure 3. Time signal at the truncation point ($x_1 = 10\lambda_R$, λ_R being the Rayleigh wavelength for the central frequency) for the free Rayleigh pulse problem. The solid line corresponds to the analytical solution. The dashed line and the circles correspond to the truncated and the corrected BEM models, respectively.

analytical solution and those of the corrected numerical method show excellent agreement for all times, as expected. Although the time signals at only two points are depicted, this agreement holds throughout the computational domain, even for the truncation point $x_1 = 10\lambda_R$. By contrast, apparent spurious reflections can be observed in the truncated solution. For $x_1 = 0.5\lambda_R$, these reflections are well separated from the physical signal, and for short times, the truncated method provides accurate results. However, for longer times, or closer to the truncation point, the truncated numerical solution is noticeably distorted. Indeed, the results in $x_1 = 10\lambda_R$ for the truncated method show an artificial amplification of the signal.

These results serve as a validation for our method. As expected, the numerically obtained values for the amplitude of the Rayleigh wave in the frequency domain $R^+(\omega_i)$, for all considered frequencies ω_i, coincide with the discrete Fourier transform of the pulse.

4.2. Transient Lamb's problem

The aluminum half-space is subjected to the action of a pulsed vertical load with Gaussian spatial distribution. The time dependence is again given by Eq. (26). The radius of the Gaussian function has been taken as $0.3\ \lambda_R$. Invoking the symmetry of the problem, only a quarter-space is analyzed with symmetry boundary conditions along the fictitious vertical boundary (see Fig. 4).

For this example, only an asymptotic analytical solution on the surface is available, which can be obtained from the solution for a concentrated load of time-harmonic dependence [13] by

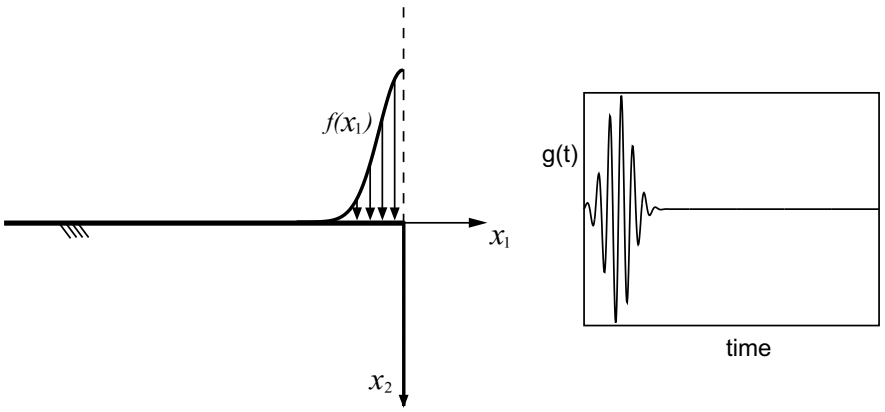

Figure 4. Schematic of Lamb's problem with Gaussian spatial distribution.

convolution in time with the pulse, and superposition in space. The distance at which the body waves have sufficiently attenuated to become negligible can be estimated given the frequency content of the signal. This guides the selection of the truncation point. Here, the truncation point on the surface is located at a distance of $60\lambda_R$ from the symmetry axis. Note that the fictitious boundary along the symmetry axis does not carry Rayleigh surface waves. Thus, the simple truncation of this boundary leads to accurate results and no correction is needed. Here, this boundary is truncated at a distance of $60\lambda_R$ from the surface.

Figures 5 and 6 show analogous results as in the previous example. The points at which the time signal is plotted are far enough from the source for the asymptotic analytical solution to be valid. Again, the corrected numerical solution shows excellent agreement with the asymptotic analytical solution, and it does so for any time and location on the computational boundary. By contrast, the truncated solution exhibits spurious reflections. In particular, for $x_1 = 60\lambda_R$, i.e. right on the truncation point, the artificial reflection interferes with the direct signal.

These examples show that, as opposed to the simple truncation, the proposed correction allows for the undamped Rayleigh waves to escape the computational domain without producing reflections from its ends, provided the truncation point is located at sufficient distance from the source region. Thus, the corrected BEM numerical solution is accurate everywhere in the computational domain and for all computed times.

5. CONCLUSIONS

A simple, elegant approach is proposed to correct the error introduced by the truncation of the infinite boundary in the BEM modelling of elastodynamic wave propagation in semi-infinite domains. The proposed method exploits the knowledge of the asymptotic behavior of the solution to adequately correct the BEM displacement system matrix for the truncated problem to account for the contribution of the omitted part of the boundary. As opposed to the infinite element approach which requires special integration schemes in general, here the reciprocity theorem of elastodynamics is invoked to express this contribution in terms

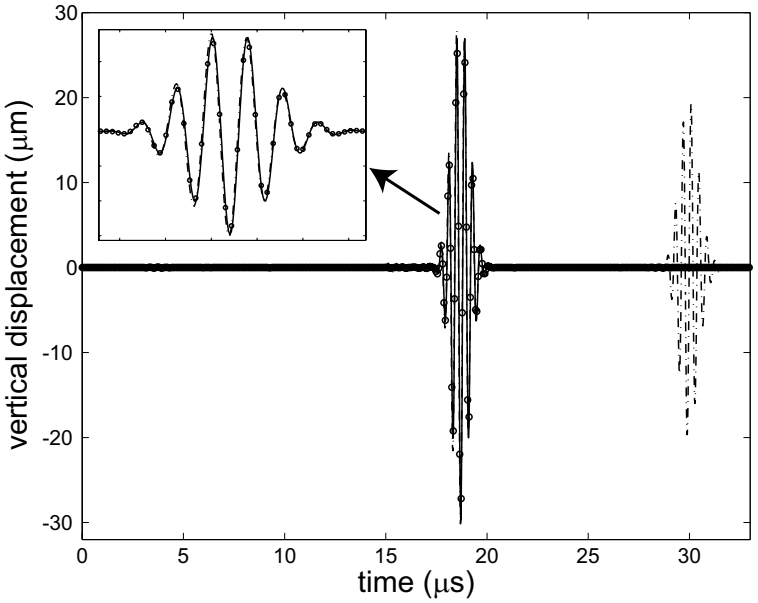

Figure 5. Time signal at $x_1 = 45\lambda_R$ (λ_R is the Rayleigh wavelength for the central frequency) for the transient Lamb's problem with Gaussian spatial distribution. The solid line corresponds to the asymptotic analytical solution. The dashed line and the circles correspond to the truncated and the corrected BEM models, respectively.

of integrals of known quantities over the discretized boundary of the domain and additional fictitious boundaries. By interpolating the far-field solution with the element shape functions, these integrals are directly obtained from the same element integrals that form the original BEM system. As a result, the proposed method is easy to implement and comes at very low additional cost as compared to the simple truncation of the boundary.

It is important to note that the additional boundaries are introduced for direct integration purposes only and do not add degrees of freedom to the final BEM system of equations. In general, the cost of computing the integrals over the additional fictitious boundaries is very low. In some particular cases, e.g. a symmetric half-space which is analyzed as a quarter-space, no additional fictitious boundary is needed and the contribution from the omitted part of the boundary is expressed in terms of integrals over the discretized boundaries only with no additional cost.

The formulation – although it can be extended to a broader range of problems – has been presented in detail in the context of the frequency domain BEM for two-dimensional elastodynamic problems for a homogeneous, isotropic, linearly elastic half-space. In this type of problems, Rayleigh surface waves propagate along the surface of the half-space without attenuation. The simple truncation of the boundary then produces considerable reflections from the end points of the domain. It has been shown through simple test examples that the proposed treatment of the infinite boundary allows the Rayleigh waves to escape the computational domain without producing spurious reflections at the end points, and it therefore eliminates the need for artificial damping. The accuracy of the solution provided by the proposed model

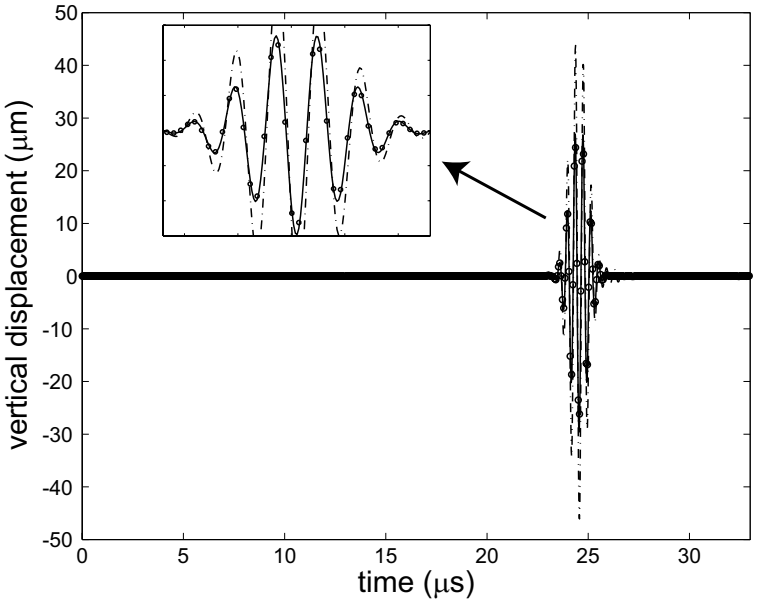

Figure 6. Time signal at the truncation point ($x_1 = 60\lambda_R$, λ_R being the Rayleigh wavelength for the central frequency) for the transient Lamb's problem with Gaussian spatial distribution. The solid line corresponds to the asymptotic analytical solution. The dashed line and the circles correspond to the truncated and the corrected BEM models, respectively.

depends on the accuracy of the assumption that Rayleigh waves strongly dominate at the end points of the computational domain. However, once the computational domain is extended far enough from the source region for this assumption to hold, then the solution is accurate everywhere in the computational domain and for all computed times. This is not the case in the truncated model, where the accuracy of the solution is degraded near the ends of the computational domain and for sufficiently long times reflections are observed at any location.

ACKNOWLEDGEMENTS

This paper is based upon work partially supported by the Federal Aviation Administration under Contract #DFTA 03-98-F-IA029, and partially supported by the Office of Naval Research under Contract N00014-89-J-1362.

REFERENCES

1. Geers TL. (Ed.) *IUTAM Symposium on Computational Methods for Unbounbded Domains*. Kluwer Academic Publishers, Dordrecht, 1998.
2. Domínguez J. *Boundary Elements in Dynamics*. Computational mechanics publications, Elsevier applied science, 1993.
3. Watson JO. Advanced implementation of the boundary element method for two- and three-dimensional elastostatics. In *Developments in Boundary Element Methods – I,* Banerjee PK, Butterfield R (eds). Elsevier Applied Science Publishers: London, 1979; 31–63.

4. Beer G, Watson JO. Infinite boundary elements. *International Journal for Numerical Methods in Engineering* 1989; **28**:1233–1247.
5. Zhang C, Song C, Pekau OA. Infinite boundary elements for dynamic problems of 3-D half-space. *International Journal for Numerical Methods in Engineering* 1991; **31**:447–462.
6. Bu S. Infinite boundary elements for the dynamic analysis of machine foundations. *International Journal for Numerical Methods in Engineering* 1997; **40**(21):3901–3917.
7. Domínguez J, Meise T. On the use of the BEM for wave propagation in infinite domains. *Engineering Analysis with Boundary Elements* 1991; **8**(3):132–138.
8. Heymsfield E. Infinite domain correction for anti-plane shear waves in a two-dimensional boundary element analysis. *International Journal for Numerical Methods in Engineering* 1997; **40**(5):953–964.
9. Heymsfield E. Infinite domain correction for in-plane body waves in a two-dimensional boundary element analysis. *International Journal for Numerical Methods in Engineering* 1997; **40**(9):1687–1700.
10. Li ZL, Achenbach JD. Interaction of a Rayleigh wave with a disbond in a material interphase normal to a free surface. *Ultrasonics* 1991; **29**(1):45–52.
11. Wheeler LT, Sternberg E. Some theorems in classical elastodynamics. *Archive for Rational Mechanics and Analysis* 1968; **31**:51–90.
12. Achenbach JD. *Wave propagation in elastic solids*. North-Holland, Elsevier, 1973.
13. Lamb H. On the propagation of tremors over the surface of an elastic solid. *Philosophical Transactions of the Royal Society (London)* 1904; **A203**:1–42.